Food Research International 130 (2020) 108921

Contents lists available at ScienceDirect

Food Research International

journal homepage: www.elsevier.com/locate/foodres

Low-energy short-term cold atmospheric plasma: Controlling the inactivation efficacy of bacterial spores in powders

M.C. Pina-Perez[a], D. Martinet[b], C. Palacios-Gorba[a], C. Ellert[b], M. Beyrer[a,*]

[a] Institute of Life Technologies, Department Natural Food Products, Route du Rawyl 64, 1950 Sion, Switzerland
[b] Institute of Systems Engineering, Route du Rawyl 47, 1950 Sion, Switzerland

ARTICLE INFO

Keywords:
Cold Atmospheric Plasma
Surface energy
Powders
Bacterial spores
Novel technologies
Food safety

ABSTRACT

The present research work aims to elucidate kinetics and mechanisms of the inactivation of *Bacillus subtilis* spores by a surface micro-discharge (SMD) - cold atmospheric pressure plasma (CAPP). Regarding industrial applications, the inactivation of spores was also studied for a static layer of a biopolymer powder or film, with an air plasma and at ambient pressure. Close to 4 $\log_{10}$ cycles of inactivation of *Bacillus subtilis* spores were achieved when exposing spores on flat glass to the SMD-CAPP. This effect can be reached at a very low plasma power density of 5 mW/cm^2 in 7 min exposure time. The maximum inactivation level of spores drops when treating corn-starch powder to 2.6 $\log_{10}$ cycles at 7 mW/cm^2 plasma power density for 5 min and with a polymer load of 5 mg/cm^2. Similar is true for films produced with hydroxymethyl cellulose (HMC). The inactivation efficacy can be tuned and is a function of applied surface energy (product of the plasma power density and the exposure time) and the polymer load. Plasma diagnostics reveal the fundamental importance of reactive nitrogen species (RNS) in the inactivation. Etching of spore hull is supposed to be triggered by the plasma density, while UV-C and UV-B radiation do not contribute directly and significantly to the inactivation effect at least in a biopolymer matrix. Fluidization of a fixed powder layer is supposed to overcome limitations of the inactivation efficacy by reducing the diffusion distance of active plasma species between the source and the sample. The combination of low plasma power density with short treatment time is supposed to reduce the risk of the formation of side-products from the matrix.

1. Introduction

A plasma is a partially ionized gas. Diverse applications on biological materials, among them, wound sterilization, pesticides degradation, wastewater treatment, and destruction of prions, mycotoxins, and microorganisms have been described (Afshari & Hosseini, 2014; Mir, Shah, & Mir, 2016; Stoica, Alexe, & Mihalcea, 2014). In food processing, cold plasma is proposed as a non-thermal technology for the preservation of liquid or solid products. However, legal aspects and the possible generation of toxic side compounds, uncertainties concerning plasma effects on nutritional or organoleptic food properties limit a rapid introduction of plasma treatments at an industrial level (Keener & Misra, 2016; Pankaj, Wan, & Keener, 2018).

Different plasma generating devices have been tested for food processing, such as corona discharge, micro hollow cathode discharge, gliding arc discharge, dielectric barrier discharge (DBD), surface microdischarge (SMD) plasma, and atmospheric pressure plasma jet (APPJ) (Bárdos & Baránková, 2010; Bußler, 2017; Kämpfl, Isbary, Shimizu, Li, Zimmermann, Stolz, Schlegel, Morfill, & Schmidt, 2012; Li, Shimizu, Zimmermann, & Morfill, 2012; (Sarangapani et al., 2018)). DBD and SMD devices offer the possibility of generating large area plasmas and upscaling to a high throughput of powder can be assumed to be easy. An SMD setup consists of two planar electrodes (one is structured or a mesh) sandwiched with an insulator plate made of ceramic, plastic, or glass. Non-charged gas species and other antimicrobial agents with a relatively long lifespan diffuse from the plasma active region in the structured mesh electrode to the sample (Bárdos & Baránková, 2010; Yi et al., 2017), whereas charged plasma species (electrons, ions) move only between the electrodes. This fact limits potential detrimental effects in susceptible materials and biological tissue related to direct plasma exposure, e.g. at processing in a DBD plasma (Isbary et al., 2013).

Plasma generation at atmospheric pressure (cold atmospheric pressure plasma, CAPP) and using air as process gas is the most preferable option for applications in food manufacturing (Shimizu, Zimmermann, & Morfill, 2015). The matrix-free microbial inactivation

* Corresponding author.
E-mail address: michael.beyrer@hevs.ch (M. Beyrer).

https://doi.org/10.1016/j.foodres.2019.108921
Received 2 September 2019; Received in revised form 10 December 2019; Accepted 15 December 2019
Available online 18 December 2019

with an SMD-CAPP is successful and a reduction of 3–7 $\log_{10}$ cycles was achieved with both, bacterial cells or bacterial spores (Jeon, Kämpfl, Zimmermann, Morfill, & Shimizu, 2014; Kämpfl et al., 2012; Yi et al., 2017). However, the decontamination of powders with a plasma is much less effective and development work is required in preparation of industrial applications (Cullen et al., 2018; Kim, Lee, & Min, 2014; Kim, Oh, Won, Lee, & Min, 2017).

Frequently studied technologies for decontamination of powders are, such as dry heating, pulsed light technology, microwave heating, and gamma irradiation. However, some important issues remain unsolved, i.e., undesired changes in the product, manufacturing costs and in some cases resistance of spores (Dababneh, 2013; Guo, 2013). These issues are driving the investigation on alternative non-thermal treatments to sterilize food powders (EFSA, 2014; Farakos & Frank, 2014), protecting valuable components and properties of powders, such as volatile flavors and vitamins, or structure in terms of particle size and flowability (Hörmansperger et al., 2016). Regarding advancements of plasma technologies, important questions to deal with are, (i) research on involved mechanisms of the inactivation of microorganisms linked to the assessment of the plasma composition, and (ii) elucidation of possible side-reactions of the matrix material or foodstuff.

The present research work aims to evaluate factors influencing the efficacy of inactivation of *Bacillus subtilis* spores with a SMD-CAPP when using static, ambient air as a process gas. The inhibiting effect of different powders will be compared to a reference and tuning factors will be validated. Insight into inactivation mechanisms at specific conditions will be provided via plasma analytics.

2. Material and methods

2.1. Microbial strains and preparation of inoculum subcultures

Bacillus subtilis D-2 was used in the present study. This strain was obtained from the culture collection of the HES-SO Valais-Wallis, Institute of Life Technologies (Sion, Switzerland).

B. subtilis endospores were transferred from stock cultures on tryptic soy agar (TSA, Biolife, Italy) and incubated for 24 h at 37 °C. Spores grown on TSA plates were harvested and bacterial suspensions were prepared on tryptic soy broth (TSB, Biolife, Italy) for 24 h with agitation at 3 × *g* at 37 °C. The spores were harvested by centrifugation at 3000 × *g* and 4 °C for 10 min and washed twice with sterile peptone water (0.85% NaCl and 0.1% neutralized bacteriological peptone). The washed spore pellets were re-suspended in 0.1% peptone water. A volume of 600 µL of each spore suspension was layered onto tryptic soy agar (TSA, Biolife, Italy) in 12 × 12 cm^2 square versions of Petri dishes and incubated for 10 days at 37 °C for sporulation. After the incubation period, sporulation was examined by phase-contrast microscopy. Spores were harvested from the surface of the culture plates rubbing the upper layer using a sterile glass spatula (97–99% sporulation after 10 days). Spore suspensions were transferred to 50 mL tubes and heated in a water bath at 80 °C for 20 min to kill any vegetative cells. Heat-treated suspensions were then centrifuged at 500 × g and 4 °C for 20 min. The pellet was re-suspended in sterile demineralized water (DMW) to a concentration of approximately 10^9 spores/mL. Routinely, spore dispersions were checked by phase-contrast microscopy for purity. The stock suspension was submitted to an additional maturation step of 1 month at 4 °C to reduce the heterogeneity of early spore population (Wallen & Walker, 1980).

2.2. Sample preparation and inoculation

Sterile flat glass (76 × 26 mm^2) was used as carrier material to expose inoculated samples to SMD-CAPP treatments. Three different matrix models were inoculated with *B. subtilis* spores and spread on flat glass to be treated by SMD-CAPP.

2.2.1. Reference model - B. subtilis spores on sterile flat glass

Liquid culture of *B. subtilis* spores in DMW was distributed (0.1 mL) on sterile flat glass and subsequently air-dried in a laminar flow cabinet overnight (N_0 = initial bacteria load in the stock CFU/mL; $\log_{10} N_0$ = 9.13 ± 0.19). Spores disposed on sterile flat glass (6.9 × 10^7 spores/cm^2) were subjected to SMD-CAPP at different treatment conditions. Two replicates in three different working sessions were used to estimate spore resistance to SMD-CAPP different treatments.

2.2.2. Powdered material

Cornstarch was used as powder matrix in the present study. An inoculum of stock suspension of spores (10^9 spores/mL) was prepared in DMW and mixed with powder using [1:1] (v/w) ratio. The mixture was homogenised and freeze-dried (final $\log_{10}$ (N_p) = 7.58 ± 0.12; N_p - spores/g powder). The contaminated powder was loaded in the range from 5 mg/cm^2 (0.1 g/19.76 cm^2) to 35 mg/cm^2 (0.7 g/19.76 cm^2) on sterile flat glass. The amount of powder was checked by weighing out before and after the treatment.

2.2.3. Film forming material

A Hydroxymethyl cellulose (HMC) solution was prepared to obtain films with embedded spores. Firstly, glycerol (2.5% (v/v)) was added to water (100 mL) and heated to 80 °C. Then, 4.7% (w/v) HMC was added while stirring and the temperature was decreased to room temperature. Mixing was continued until a clear solution was obtained. The solution rested 3 h without agitation to ensure the elimination of air bubbles. Solutions were inoculated with *B. subtilis* spores (to a final concentration of 10^7 CFU/mL). Film-forming solutions were spread onto sterile glass plates and dried in a laminar flow box at room temperature. Film composition and preparation protocol was selected based on final suspension viscosity, film quality, and the survival rate of inoculated bacteria (97%). HMC films (5, 10, 24, 35, 60, 83 mg/cm^2 HMC load; thickness in the range 35 ± 5 µm to 145 ± 12 µm) were peeled from the plates, cut, and adapted to flat glass size to be treated by SMD-CAPP. HMC films were characterized for the (%T) transmittance of UV-light (200–400 nm) using a UV–VIS spectrophotometer (Thermo Scientific, SA).

2.3. Surface microdischarge (SMD) plasma equipment configuration

Tailor-made SMD equipment was built by the Institute of Systems Engineering (HES-SO Valais-Wallis, Sion, Switzerland). A high-voltage powered mesh electrode (mesh size = 9.8 × 9.4 mm), a Teflon dielectric sheet, and a planar electrode were mounted together without gap. The grounded planar electrode was made of aluminum mounted with a stainless-steel powered mesh electrode (see Fig. 1A). The surface of the rectangular device is 149.76 cm^2.

Samples were positioned at 6 mm distance from the mesh electrode. No agitation method was applied. The “active plasma volume” corresponds to 89.85 cm^3.

Electrical power was supplied by a function generator, a Titan™ Series (Compact Power Company, USA) low frequency power amplifier (45 Hz – 15 kHz, max. power output 130 V/8A or 1 kW) connected to a custom designed high voltage transformer (used at 6.4 – 7.4 kV peak to peak voltage) with 2–20 kHz bandwidth (Swiss Trafo Josef Betschart AG, Switzerland). A gap of 6 mm between the sample and the SMD plasma active region was maintained. When the mesh electrode was powered, many filamentary discharges with a length of up to a few millimeters formed between the dielectric and the planar electrode along the rectangular openings. The surface microdischarge (SMD) plasma emits purple light (see Fig. 1B) that is dominated by the excitation of nitrogen molecules of ambient air. The plasma was observed to be stable and uniform before sample treatment for each specific condition applied (power level – treatment time).

The device was operated at atmospheric pressure using ambient air as working gas without an active gas flow. A cooling system was

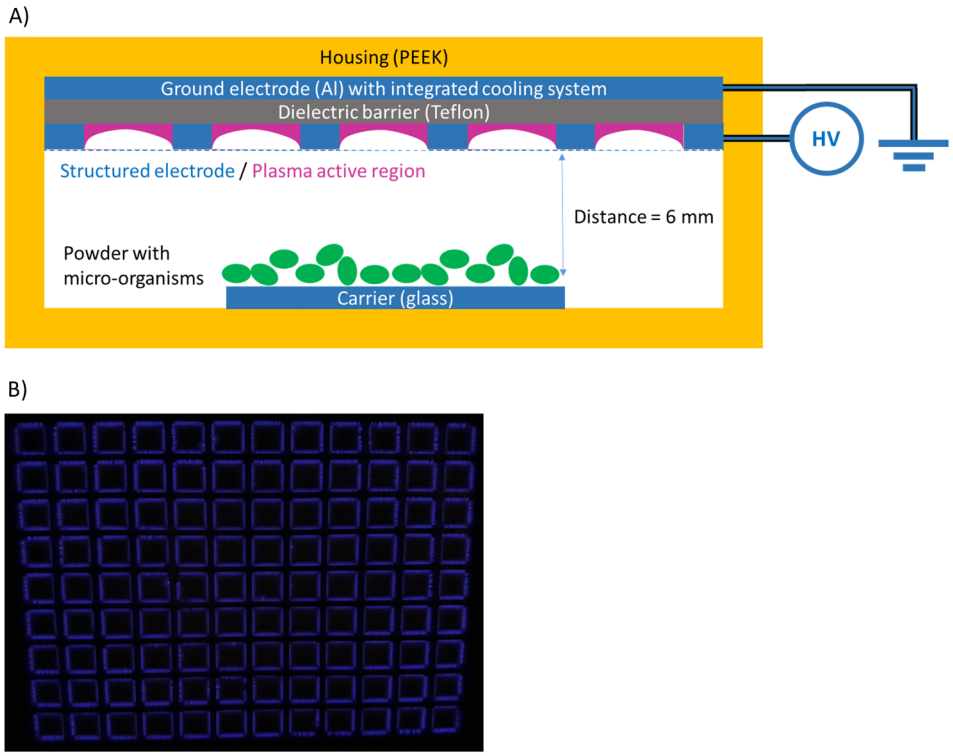

Fig. 1. Surface-microdischarge (SMD) plasma device – schematic (A) and, mesh electrode (B) partially filled with air plasma (plasma power density = 7 mW/cm^2, f = 10 kHz, V = 6.8 kV peak-to-peak value).

installed in the upper grounded electrode to prevent the heating of the dielectric barrier.

Home-made HES-SO Valais-Wallis equipment, as well as previously designed SMD devices (Wang, Doona, Setlow, & Li, 2016), can work at constant temperature close to 30 °C during treatment times between 0 and 30 min. Consequently, thermal effects in the present study are excluded as possible causes for the microbial inactivation.

Testec HVP 15 HF (Testec Elektronik GmbH, Germany) and Sapphire HV 7000 APW6 70 MHz (Sapphire Instruments Co., Ltd., Taiwan) voltage probes and Pearson model 4100 and model 110 (Pearson Electronics, Inc., USA) current probes were used to measure the power input and output of the transformer with a 500 MHz Oscilloscope (Teledyne LeCroy, USA). To determine the discharge power, the current and the voltage responses were measured in the secondary circuit as a function of time.

The power is determined by the mean value over a period T of the current multiplied by the voltage, an operation which is performed directly by the LeCroy oscilloscope:

$$P = \frac{1}{T}\int_0^T U(t) \times I(t)dt \quad (1)$$

As the current and the voltage were measured at the secondary side of the transformer, equation (1) gives the total electrical power dissipated in the plasma reactor, which is the sum of the discharge power and the power dissipated in the electrode circuit, including the dielectrics: $P_{total} = P_{discharge} + P_{circuit}$. Since the discharge current is represented by the current peaks, which are superposed on the sinusoidal current, the sine component of the current trace must be subtracted to obtain the (effective) discharge current as a function of time (Fig. 2). Eq. (1) applied to this real discharge current trace gives the power consumed in the discharge. The power values obtained with this method were corroborated with the calculation of the area of the charge-voltage curves (not shown), usually referred as the Lissajous-method (Brandenburg et al., 2008).

Experiments were carried out at 10 kHz and applying three

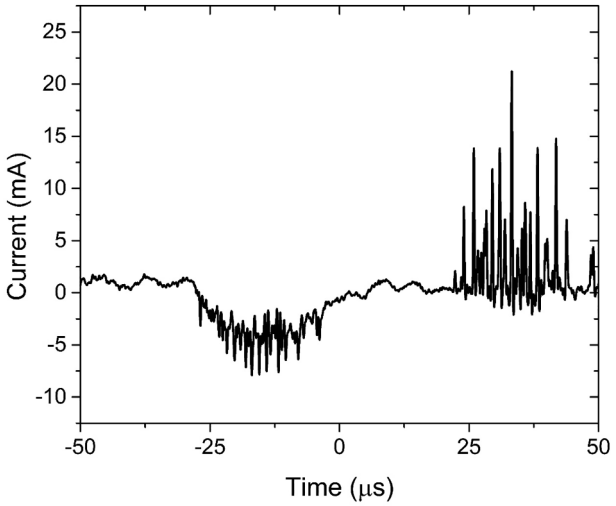

Fig. 2. Discharge current represented by current peaks. The calculation of the discharge power is based on the discharge current (Eq. (1)).

discharge power levels of 0.8 W (6.4 kV_{pkpk}), 1.1 W (6.8 kV_{pkpk}) and 1.3 W (7.4 kV_{pkpk}), corresponding with plasma power densities of 5 mW/cm^2, 7 mW/cm^2 and 10 mW/cm^2, respectively.

Samples prepared according to Section 2.2 were introduced in the SMD-CAPP plasma setup and submitted to treatment during controlled times. Treatment times in the range of 0.5–7 min were used for each discharge power level applied. Flat glass with deposited spores, contaminated cornstarch powder, or HMC films, without plasma treatment were used as control samples at each working session (treatment time = 0 s). Experiments were conducted at room temperature and each test was performed in triplicate.

For the optical emission spectroscopy (OES), two different spectrometers were used: a UV – visible light spectrometer, ranging from

340 to 1020 nm (USB 2000, Ocean optics, USA) and an UV light spectrometer, ranging from 200 to 420 nm (MayaPro 2000, Ocean Optics, USA). For both spectrometers, a UV-grade optical fiber of 400 μm core diameter and 1 m length was used. The spectra were recorded 5 times with an integration time of 30 s and then averaged to increase the signal-to-noise ratio.

2.4. Microbiological analysis

Plasma treated samples and controls were transferred aseptically into 114 mm × 230 mm transparent sterile stomacher plastic bags (Carl Roth, Germany) immediately after the treatment and keep at 4° C until serial dilution procedure (less than 2 h). Ten mL of sterile 0.1% peptone water was added, and the bags were sealed. The samples were agitated in a stomacher blender (Stomacher Lab Blender Model 400, Seward Medical, London UK), for 1 min. Then the glass slides were removed using sterile tweezers. Spore dispersions were serially diluted in buffered peptone water 0.1% (Sigma Aldrich, SA, Switzerland), and plated in TSA. The plates were incubated at 37 °C and the colony-forming units (CFU) were counted after 24 h. This procedure was performed in triplicate and microbiological counting of each replicate was done in duplicate.

2.5. Modelling B. subtilis inactivation kinetics under SMD-CAPP treatment

The inactivation effect, at each plasma density level applied, is described by the decimal logarithm of the ratio of the final and initial spore concentration (N_t and N_0 respectively).

Inactivation kinetics were fitted to a first order approach according to Eq. (2),

$$log_{10}\frac{N_t}{N_o} = -k \times t = \frac{-t}{D} \quad (2)$$

where D (s) = 1/k is the decimal reduction time.

Additionally, kinetic inactivation curves for each plasma density level were fitted to the Weibull distribution function (3)

$$log_{10}\left(\frac{N_t}{N_0}\right) = -\left(\frac{t}{b}\right)^n \quad (3)$$

where the parameter n is the shape parameter, and b *(s)* is the scale parameter and represents the mean of the distribution describing the death times of the microbial population. Values of the shape parameter close to 1 are characteristic for linear curves. The shape parameter also accounts for upward concavity of a survival curve for $n < 1$, and downward concavity for $n > 1$. A value of $n < 1$ indicates that the remaining cells can adapt to the applied stress, whereas $n > 1$ indicates that the remaining cells become increasingly damaged (Pina-Perez, Silva-Angulo, Muguerza, Rodrigo, & Martinez, 2009).

2.6. Recovery of sublethally damaged spores after SMD-CAPP: Mathematical modelling of outgrowth

Surviving spores after SMD-CAPP treatment can remain damaged, or retaining the capacity to germinate, repair damage, and grow out (Setlow, 2007; Warda, Tempelaars, Abee, & Nierop Groot, 2016). To further demonstrate how plasma dosage can be related with spore affectation, germination dynamics of surviving spores (damaged/not damaged) and subsequent growth of vegetative cells after SMD-CAPP treatments (5–10 mW/cm^2, treatment time 0–5 min) was evaluated.

On flat glass slides treated spores were transferred into 114 mm × 230 mm transparent sterile stomacher plastic bags. Ten mL of TSB were added, and the bags were sealed. The samples were agitated in a stomacher blender for 1 min. Then the glass slides were removed using sterile tweezers and the spore dispersions were serially diluted on sterile TSB tubes up to an optical density (OD) value of 0.1 measured at 600 nm to start after-treatment growth studies. TSB-spore dispersions were incubated at 37 °C (agitation 3 × *g*). $OD_{600\ nm}$ registration was carried out for 48 h. In parallel periodical microbiological analysis of extracted aliquots (0, 3, 6, 12, 15, 24, 28, 30, 48 h) was done. Trials were repeated in triplicate for each treatment condition. Obtained growth data were fitted to the Gompertz equation (Silva-Angulo et al., 2015; Zwietering, Jongenburger, Rombouts, & Van't Riet, 1990):

$$\log_{10}(N_t) = A + C\exp(-\exp(-B(t - M))) \quad (4)$$

where N_t represents the number of microorganisms at time t (CFU/mL); A represents the inferior asymptote value ($\log_{10}$ (CFU/mL)); C represents the difference between the curve asymptotes ($\log_{10}$ (CFU/mL); B represents the relative growth rate when t = M (($\log_{10}$ (CFU/mL))/h); M represents the elapsed time until the maximum growth rate is reached (h).

Parameters *A, B, C*, and *M* were used to calculate the lag time (λ; h), maximum growth rate (μmax) (($\log_{10}$ (CFU/mL))/h), and generation time (Gt, h) using the equations described by Gibson, Bratchell, and Roberts (1988).

2.7. Statistical analysis

All data were statistically analyzed (ANOVA) with Statgraphics Centurion XVII (Statpoint Technologies, Inc., USA) to determine the significance (p-value ≤ 0.05) influence of studied factors on inactivation as well as significant differences between SMD-CAPP inactivation levels.

3. Results and discussion

3.1. Inactivation kinetics of Bacillus subtilis spores exposed to SMD-CAPP

B. subtilis spores deposited on a flat glass were treated by SMD-CAPP at different discharge power levels, 0.8 W, 1.1 W, and 1.3 W, corresponding to plasma power densities of 5, 7, and 10 mW/cm^2, respectively. Initial spore concentration was reduced close to 1 $\log_{10}$ cycle in < 2 min, achieving 4 $\log_{10}$ cycles inactivation in just 7 min with a plasma power density of 5 mW/cm^2. To our knowledge, this is the third report achieving 3 $\log_{10}$ cycles or higher of inactivation of *Bacillus* spp. spores by SMD-CAPP in a time frame of up to 5 min, using air as process gas. The study of Wang et al. (2016) reported an inactivation of 5 $\log_{10}$ cycles for *B. subtilis* spores exposed on glass slides to a SMD-CAPP with a plasma power density of 40 mW/cm^2 during 3 min. Kämpfl et al. (2012) achieved a similar reduction of *Geobacillus stearothermophilus* and *Bacillus* spp. spores applying a plasma power density of 35 mW/cm^2 for 5 min. In the current study, the plasma power density was a magnitude lower for achieving similar inactivation levels with bacterial spores. Kämpfl et al. (2012) inactivated the microorganisms with a similar SMD-CAPP and Wang et al. (2016) applied a DBD-CAPP. In a DBD-CAPP the microorganisms are exposed directly to the plasma, while in an SMD-CAPP a distance to the plasma ignition spot exists and the exposure is semi-directly. Only in the present work, the plasma power density was calculated from the discharge (efficient) power (see Section 2.3). An electrode acts as a capacitance and not the total electric power can be transformed into discharges. At least for meaningful comparison, data on reaction kinetics should be linked most preferable to the discharge (efficient) power.

B. subtilis inactivation curves are shown in Fig. 3. Semi-logarithmic inactivation curves have a linear shape and were fitted with a 1st order reaction approach (see Table 1). Previously, Hong et al. (2009) and Jeon et al. (2014) obtained linear inactivation curves for bacterial spores when samples were exposed to an atmospheric pressure plasma. Decimal reduction times of *B. subtilis* spores (D-values) spread and reach values of 18 s, 35 s, 48 s and 1.33 min for a SMD plasma (35 mW/cm^2; 1 kHz frequency) (Kämpfl et al., 2012), a microwave excited surface

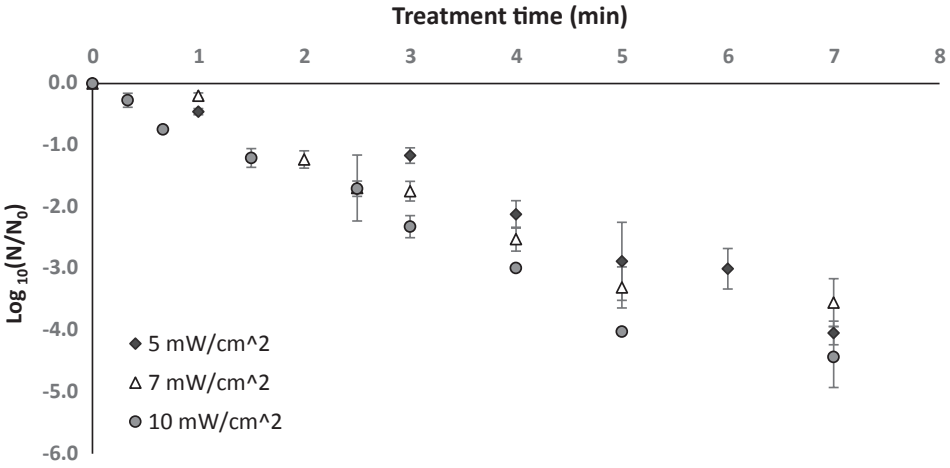

Fig. 3. Inactivation of *Bacillus subtilis* spores deposited on flat-glass by an air SMD-CAPP.

wave plasma discharges (700 W) (Singh, Ogino, & Nagatsu, 2009), a DBD diffuse glow plasma (Boudam et al., 2006), and the here presented SMD plasma (10 mW/cm^2; 10-kHz frequency), respectively. Differences of these D-values might be reasoned amongst others by differences of the applied plasma power density. A more specific comparison is not practicable, as the surface or volume-specific, efficient electric power input was not reported in many cases. However, the applicability of 1st order kinetics is supposed to be restricted to a certain inactivation phase. The rate of inactivation has been reported to slow down at extended treatment time of spores with a plasma jet (Hertwig et al., 2015).

The D-values and the plasma power density are negatively correlated. The D-values decrease from 1.8 min at 5 mW/cm^2 to at least 1.3 min at 10 mW/cm^2 (Table 1). The generalized approach is based on a representation of the inactivation effect as a function of the main driving force of the inactivation which is the product of the plasma power density and the exposure time. This product is the applied surface energy E_s in J/cm^2. For one-phase, 1st order kinetics the inactivation effect $\log_{10}$ (N_t/N_0) equals to:

$$log_{10}\left(\frac{N_t}{N_0}\right) = k_1 \times E_s + E_{s,c} \quad (5)$$

The slope of the curve k_1 characterizes a rate of inactivation at the observed phase of reaction and the critical surface energy $E_{s,c}$ the minimal surface energy to apply for initiating the inactivation. With the present data for all plasma power density – exposure time combinations up to 6 min exposure, the rate of inactivation k_1 is -1.54 cm^2/J and critical energy is 0.07 (J/cm^2). The coefficient of determination is 0.95 for this example.

The inactivation curves of *B. subtilis* spores for different plasma power densities were also fitted to the Weibull distribution function. The obtained Weibull shape parameter (n) is close to 1. Fits applying 1st order kinetics or the Weibull distribution function are comparable in quality for the inactivation of *B. subtilis* spores by a SMD-CAPP (Table 1) and there is no clear preference for one of the models.

Mendes-Oliveira, Jensen, Keener, and Campanella (2019) used a DBD plasma for inactivation of *B. subtilis* spores and found a bent semi-logarithmic inactivation curve also considering inactivation's higher than 5 $\log_{10}$ cycles. It was evidenced that non-linear survival kinetics fitted with the Weibull model are not satisfying assuming the driving force is constant. The ozone was assumed being the key reactive gas and the concentration increased with the exposure time. A modeling approach using time-varying concentrations was successfully applied to experimental data and provide better fits than a traditional approach using an average concentration. Modeling bent inactivation curves requires the introduction of a secondary reaction constant k_2 into Eq. (5) still combined with the surface energy. For the presented data this is not required. The approach will be reported by the authors elsewhere. Hertwig et al. (2015) applied a similar approach for a biphasic inactivation of *B. subtilis* endospores but consider the reaction as time and not surface energy depended.

Mechanisms potentially involved in inactivation of spores by cold plasmas are (Boudam et al., 2006; Fiebrandt, Lackmann, & Stapelmann, 2018; Huang et al., 2019; Raguse et al., 2016):

(a) **photo-oxidation** of the protein coat of endospores triggered by UV radiation (200–400 nm);
(b) **etching** or "atom by atom erosion" of the protein coat and the peptidoglycan cortex (i.e. cracks and fissures) and increase of the hull's permeability triggered by reactive oxygen and nitrogen species (ROS, RNS);
(c) diffusion of ROS and RNS deeply into the spore, and irreversible **alteration of the cytoplasmic membrane, metabolic proteins, and DNA**.

The most relevant mechanisms of the inactivation of *Bacillus* spores by an SMD plasma will be distinguished in section 3.3 (plasma diagnostics).

Table 1
Kinetic parameters characterizing the inactivation of *Bacillus subtilis* spores by an air SMD-CAPP. The fit parameter D was calculated accordingly to equation (2); b and n were calculated accordingly to equation (3).

Plasma power density	D-value (min)	R^2-adjusted	RMSE	b	n	R^2-adjusted	RMSE
5 mW/cm^2	1.8 ± 0.06	0.977	0.050	2.20 ± 0.15	1.19 ± 0.05	0.986	0.037
7 mW/cm^2	1.6 ± 0.03	0.960	0.067	1.92 ± 0.12	1.30 ± 0.15	0.984	0.027
10 mW/cm^2	1.3 ± 0.02	0.988	0.021	1.24 ± 0.11	0.94 ± 0.08	0.991	0.018

RMSE: Root Mean Square Error; b Weibull scale parameter; n Weibull shape parameter.

Table 2
Germination of sublethal damaged spores of *Bacillus subtilis* and growth of vegetative cells as a function of the plasma power density calculated accordingly to the Gompertz equation: lag phase duration (T_{lag}, h) and maximum specific growth rate ($\log_{10}$ μ_{max}; CFU/mL/h) after a plasma exposure time of 300 s.

Plasma treatment	T_{lag} (h)	log μ_{max}, (CFU/mL/h)	R^2-adjusted	MAE
Untreated spores	4.8 ± 0.23[a]	0.24 ± 0.04[a]	0.977	0.041
5 mW/cm^2	9.2 ± 0.14[b]	0.20 ± 0.01[b]	0.997	0.017
7 mW/cm^2	9.7 ± 0.25[b]	0.21 ± 0.01[b]	0.997	0.014
10 mW/cm^2	12.0 ± 0.25[c]	0.19 ± 0.02[b]	0.998	0.011

[a-b]: different superscript letters are indicating significant differences (p-value < 0.05) per column according to an ANOVA analysis; MAE: Mean Absolute Error.

3.2. Sub-lethal damage and repair capacity of surviving B. subtilis spores after SMD-CAPP

A sub-lethal damage and subsequent repair mechanism is supposed to influence the dynamic of growth of *B. subtilis* spores. The lag-phase of outgrowth (T_{lag}) and the maximum specific growth rate (μ_{max}) vary significantly between non-treated and treated cells. Besides, T_{lag} increases with the applied plasma power density (see Table 2). The surviving population of spores needs more time for successfully repairing damages at higher plasma power densities, but once the spores germinate, the growth rate of vegetative cells is similar.

Wang et al. (2016) revealed that T_{lag} of *B. subtilis* spores increased with the SMD-CAP treatment time and plasma density. The dipicolinic acid (DPA) depot of irreversible damaged spores depleted. Morphological modifications of *B. subtilis* spores, such as shrinkage in size, rupture of the spore membrane, and leakage of the cytoplasm, have been also observed as a result of a DBD plasma exposure (Deng, Shi, & Kong, 2006). Huang et al. (2019) described an erosion effect at the coat of spores while the intensity of the DBD plasma treatment controlled the erosion effect. According to Wang et al. (2016) the degradation of the spore structure and inactivation of proteins which are essential for germination are closely related. While a sub-lethal damage is rather driven by spore coat modifications, a subsequently increasing permeability might be a key factor of lethal impact (Boudam et al., 2006; Wang et al., 2016). The linear shape of the inactivation curve in a semi-logarithmic plot does not indicate a change of the inactivation mechanism during the treatment time (see Fig. 3). Plasma diagnostics combined with inactivation kinetics give more evidence on inactivation mechanisms.

3.3. Plasma diagnostics and inactivation mechanisms

Plasma chemistry is highly dependent on the composition of the feeding gas, the configuration of the setup and further operation conditions. To get insight into the composition of a SMD-CAPP, the optical emission spectrum (OES) was registered at 6 mm distance from the source (corresponding with the position of the samples). No emission of UV-C (200–280 nm) or UV-B (280–315 nm) was detected. UV-C will be absorbed in air at atmospheric pressure over 1.5 mm distance (Denny, 1993). Already due to the distance of the sample to the plasma source (6 mm), UV-C radiation will not reach the sample and will therefore not contribute to the inactivation effect. Plasma diagnostics as presented by Wang et al. (2016) for a SMD-CAPP (60 kHz; 14 kV peak-to-peak value; 35 mW/cm^2) confirm the absence of UV-C and UV-B. In conclusion, a direct photo-oxidation of the protein coat is not considered to be the dominant inactivation principle in the herein described SMD setup.

The OES is dominated by N_2 species of the second positive system (320–400 nm), corresponding to UV-A (Fig. 4). Three major emission peaks were detected at 337 nm, 357 nm, and 380 nm, representing the major bands of the N_2 (C) excited state of the N_2 molecule. A minor peak was detected at 391 nm, corresponding to the trace of ionized nitrogen (N_2^+). The presence of O_3 was not evidenced (800–1000 nm). Similar OES results were reported by Kämpfl et al. (2012) and Hertwig, Reineke, Rauh, and Schlüter (2017). An explanation for this observation is that ozone might react immediately with highly concentrated reactive nitrogen species (RNS), and generates NO, NO_2 or NO_3, among others. Consistently, Shimizu, Zimmermann, & Morfill (2015) described a high NO_x concentration combined with a low O_3 concentrations for a SMD-CAPP. In such a situation, the rate of O_3 generation would be lower than the loss rate, leading to a low, or not detectable ozone signal in the OES. Yi et al. (2017) reported on variable processing time depended ozone generation and loss rates. However, it cannot be concluded from a low O_3 concentration or a high O_3 turnover rate, respectively, that O_3 is insignificant for the inactivation of spores.

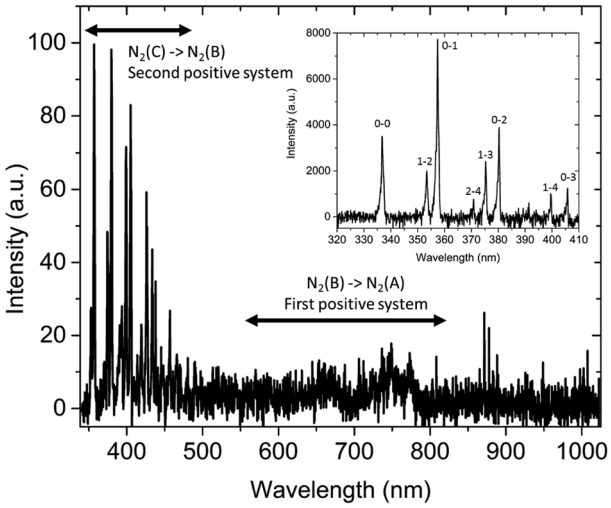

Fig. 4. Optical emission spectrum (320–1020 nm) of SMD-CAPP generated with static air. The inset shows a detailed zoom in the UV-light spectrum 320–410 nm (Second positive system of nitrogen), with an indication of the vibrational levels of the transition.

Obviously, RNS and most probably also ROS, contribute to the inactivation of endospores from *B. subtilis* (Hertwig et al., 2017; Surowsky, Schlüter, & Knorr, 2014). At a high turnover rate of ROS, and O_3 specifically, the importance of RNS is estimated to be over this of ROS. The diffusion of reactive species is time-dependent, and the sample is placed at 6 mm distance to the source. RNS triggered "etching" of the coat and cortex is thought to be the basic principle of inactivation of endospores of *B. subtilis* at exposure to a semi-direct plasma, such as an SMD plasma (Boudam et al., 2006; Singh et al., 2009).

To elucidate the dose-effect relation, the discharge power was varied in the range 0.6–2.2 W (5–15 mW/cm^2 plasma power density). An increment in the plasma power density is positively related to the intensity of N_2 bands of the second positive system (Fig. 5). In addition, the discharge power is positively related to the sporicidal effect (5 mW/cm^2, 5 min, 3 $\log_{10}$ reduction; 10 mW/cm^2, 5 min, 4 $\log_{10}$ reduction). Wang et al. (2016) observed an alteration of the coat structure of spores that is associated to the plasma density. In conclusion, the main dose-effect relation is assumed to be based on the concentration of RNS and in combination with an assumed O_3 generation, consequently also NO_x.

Chemical reactions of RS with the coat of spores, leading to an increase in the coat permeability and might continue with a diffusion of RNS into inner spore compartments. The consequence might be an alteration of metabolic proteins or genetic material. In this study, a constant formal reaction rate over the exposure time of up to 7 min was detected (see Fig. 3, Table 1). An intermediate change of the inactivation principle is unlikely. In conclusion, etching of the spore hulls is most likely the dominant inactivation principle.

Immersing spores into bio-polymers gives further information on

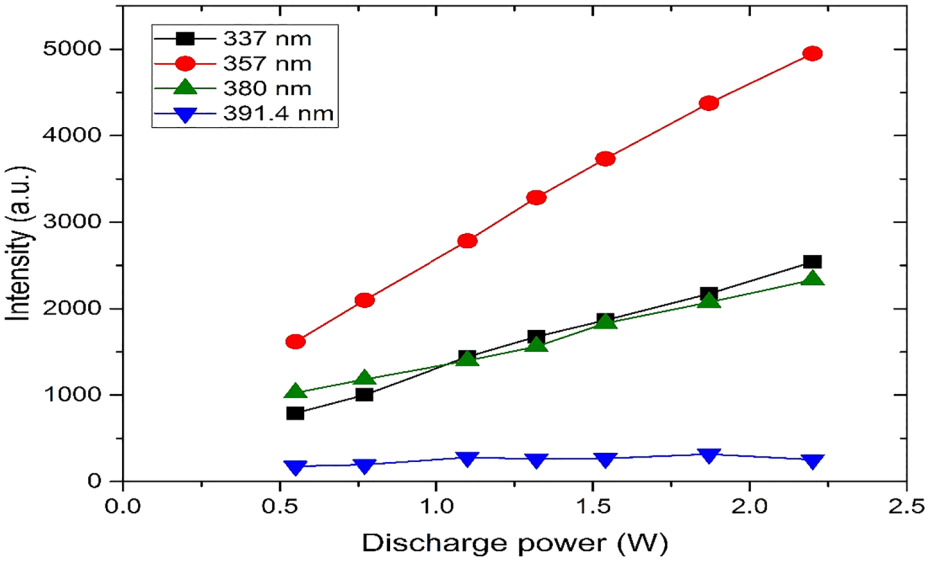

Fig. 5. Intensity of nitrogen bands as a function of discharge power.

inactivation principles and data on inactivation kinetics in a real food matrix.

3.4. *Bacillus subtilis* inactivation in a biopolymer matrix

The adequate inactivation of bacterial spores by plasma in food powders, such as onion powder, spices, red and black pepper, or legume flour, request a higher plasma power density and longer treatment time compared to a matrix-free inactivation on flat glass carriers (Hertwig et al., 2017; Kim et al., 2014, 2017; Mosovská et al., 2018). In the present case-study, contaminated corn-starch was loaded with 5 mg/cm^2 on flat glass. In comparison to an exposure of spores on flat glass carriers, in cornstarch powder the SMD-CAPP inactivation effects were significantly reduced, e.g., 1.3 $\log_{10}$ cycles less reduction with corn-starch compared to the reference at 7 mW/cm^2, 5 min (see Table 3). Wheat flour and black pepper powder reduced the inactivation of *Bacillus* spp. spores by UV light (1.63 W/cm^2) by 2 $\log_{10}$ cycles compared to a matrix-free exposure at the same exposure time (Fine & Gervais, 2004). Any matrix might influence the plasma efficacy by shadowing.

Loading the glass carriers with increasing amounts of contaminated cornstarch (5 to 35 mg/cm^2) and submitting the samples to a SMD-CAPP treatment at 7 mW/cm^2 for 5 min, resulted in a decrease of the inactivation effect (Fig. 6). Moreover, the increase of the powder load by a factor 6 resulted in a decrease of the inactivation by a factor 100. The trend was confirmed for protective effects produced by hydroxymethyl cellulose (HMC). HMC films were obtained by gentle drying of aqueous HMC-spore dispersions. Films with 5, 10, 25, 35, 60, 85 mg DM/cm^2 were SMD-CAPP treated. Selected inactivation effects are reported in table 4. The inactivation levels achieved on cornstarch powder and in HMC films are insignificantly different (p-value $\leq$ 0.05) for the same polymer load: 5 mg/cm^2 and 25 mg/cm^2.

Specifically, when upscaling a plasma device, observed ratios of powder load and inactivation of bacteria influence dimensioning of the electrode surface. For an optimization of the exposure of the sample surface fluidization systems have been applied, e.g. a vibrating table in a DBD plasma for the treatment of sprout seeds (Butscher, Zimmermann, Schuppler, & Rohr, 2016), modification of the flow rate of the ignited gas (plasma jet) through a packed bed of milk powder (Chen et al., 2019) or oscillation of the carrier of pepper grains immersed in a diffuse coplanar surface barrier discharge plasma (Mosovská et al., 2018). Such improvements are supposed to be related to the particle size and further surface properties; while in wheat grains the agitation do not improve the inactivation effect (Butscher et al., 2016), a limited improvement (1.5 $\log_{10}$ cycles of reduction of *B. subtilis* spores) was observed for pepper grains (Mosovská et al., 2018) and clear improvements were obtained with increasing flow rates when inactivating *Cronobacter sakazakii* in milk powder (Chen et al., 2019). HMC forms porous films, while starch granules form a fixed bed. In both cases, the dry matter load or thickness is crucial for the inactivation effect. A reduction of the layer thickness is an alternative to an agitation system, specifically in plasma processing of micro-particles such as starch or milk powder particles.

Table 3
Bactericidal effect ($\log_{10}$ (N/N$_0$)) of SMD-CAPP against *Bacillus subtilis* spores exposed on flat glass and in cornstarch (powder load = 5 mg/cm^2). Plasma power density = 5, 7, or 10 mW/cm^2; treatment time = 300 s.

SMD-CAPP treatment	5 mW/cm^2	7 mW/cm^2	10 mW/cm^2
Spores on flat glass	3.3 ± 0.6	3.3 ± 0.3	4.0 ± 0.1
Spores in cornstarch	1.1 ± 0.3	2.6 ± 0.1	3.3 ± 0.1

The UV light transmittance of HMC films was measured in the range 190–490 nm (Fig. 7) and is of specific interest for a wavelength of 320 nm and higher. Maximum inactivation levels (2.71 to 3.78 $\log_{10}$ cycles at 7 to 10 mW/cm^2, 5 min) were observed for HMC films with the maximum transmittance of UV-light (5 mg/cm^2 polymer load). In the range of 320–400 nm the transmittance for 5 mg/cm^2 HMC films was corresponding to 70% and was reduced to 40% for 25 mg/cm^2 HMC films. The inactivation effect gets reduced by an over proportional amount (compared to the reduction of the transmittance), i.e., by a factor of 10 and 100 for 7 mW/cm^2 and 10 mW/cm^2, respectively (Table 4). This is a clear indication, that UV light at that wavelength range is not the main trigger of inactivation, but rather, the biopolymer efficiently blocks reactive plasma species. Polymer loads higher than 25 mg/cm^2 result in an only slightly lower inactivation (1.02 ± 0.16 $\log_{10}$ cycles at an HMC load of 35 mg/cm^2) at 7 mW/cm^2 and levels out at even higher HMC loads (60 or 85 mg/cm^2). A residual inactivation of about 0.5–1.0 $\log_{10}$ cycles for high powder loads with cornstarch or HMC is thought to be related to spores that are deposited on or next to the surface of the polymer layers. The plasma blocking effect of both biopolymers is independent of the difference of the morphology (powder and film, both are porous materials) and is possibly associated with a multiple lower diffusion rate of reactive plasma species in the biopolymer layer compared to the diffusion rate in the process gas.

The inactivation effectiveness of SMD-CAPP plasma in powder can

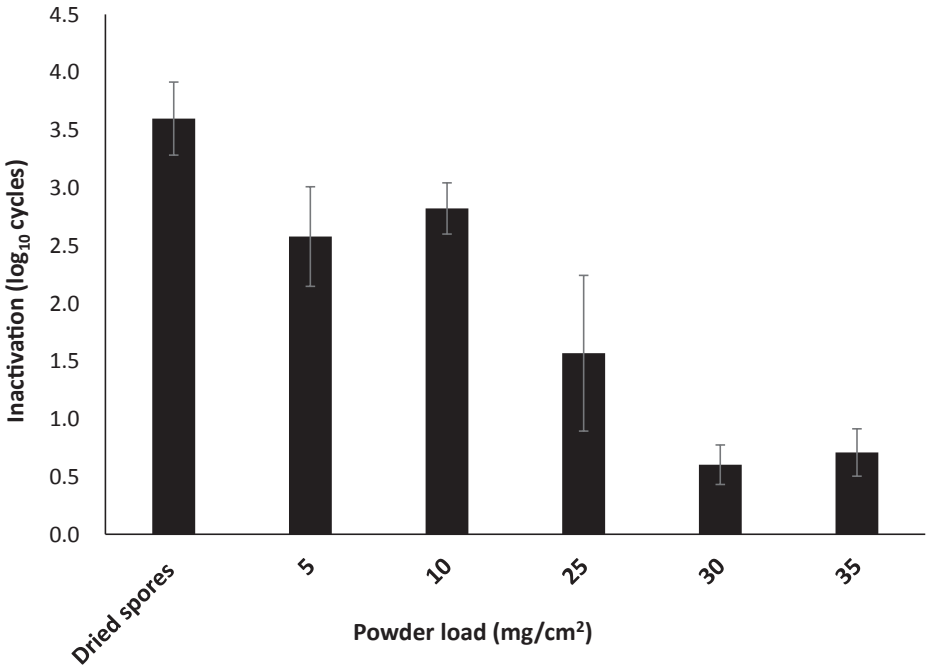

Fig. 6. Effect of the powder load on the inactivation of *Bacillus subtilis* spores deposited on cornstarch (plasma power density = 7 mW/cm^2, treatment time = 300 s).

Table 4
Inactivation of *Bacillus subtilis* spores ($\log_{10}$ (N/N_0)) in cornstarch and Hydroxymethyl cellulose (film) because of an exposition to a SMD-CAPP: plasma power density = 7 or 10 mW/cm^2, exposure time = 300 s.

Plasma power density 7 mW/cm^2		
Matrix model	Powder load	Inactivation
Spores on flat glass	0	−3.3 ± 0.3
Cornstarch	5 mg/cm^2	−2.6 ± 0.3
Cornstarch	25 mg/cm^2	−1.6 ± 0.7
HMC film	5 mg/cm^2	−2.7 ± 0.3
HMC film	25 mg/cm^2	−1.7 ± 0.8
Plasma power density 10 mW/cm^2		
Matrix model	Powder load	Inactivation
Spores on flat glass	0	−4.0 ± 0.3
Cornstarch	5 mg/cm^2	−3.3 ± 0.8
Cornstarch	25 mg/cm^2	−1.1 ± 0.1
HMC film	5 mg/cm^2	−3.8 ± 0.1
HMC film	25 mg/cm^2	−1.3 ± 0.7

be tuned by increasing the plasma power density. A moderate increase of plasma power density by a factor of 1.4 (7–10 mW/cm^2) increased the inactivation effect by 0.7 $\log_{10}$ cycles and thus by a factor of 5 or higher for a 5 mg/cm^2 layer of cornstarch or HMC. Contrary, inactivation tuning via the plasma power density failed with a polymer layer of 25 mg/cm^2 or higher. This observation supports the assumption of a dominant limitation of the inactivation effect by a low rate of diffusion of active species through the biopolymer layer.

The local concentration of SMD-CAPP species and thus the inactivation potential for spores in biopolymer layers depends on: (i) the diffusion coefficients of plasma species in the gas and the biopolymer layer, (ii) the plasma power density applied, (iii) the life span (ns, µs, ms) of active species in gas, (iv) the distance of the sample to the SMD-CAPP source, and (v) the treatment time. In the biopolymer layer, it is assumed that the rate of diffusion of SMD-CAPP generated RS is much lower than in gas, and only long-lived RS ($NO^{\bullet}$; $OH^{\bullet}$; metastable nitrogen; singlet oxygen $^1O_2$) (Shintani, 2015) are going to be able to penetrate the powder layer in depth. Such complex mass transfer problems for plasma-biopolymer layers have not been studied in detail yet. Not only the reduction of the powder load but also the fluidization of a powder layer might assist to overcome limitations of the inactivation effect by a slow-going diffusion of reactive species in porous materials.

4. Conclusions

At already very low plasma power density of 5 mW/cm^2 an inactivation of *Bacillus subtilis* spores by 4 $\log_{10}$ cycles can be achieved within 7 min of treatment time. The plasma power density was calculated from the discharge power. Description of inactivation effects as a function of the product of plasma power density and treatment time or the surface energy, respectively, is more general and delivers a function for scaling of the process.

Damages of the coat of spores and other sub-lethal modifications are repairable for a minor percentage of SMD-CAPP exposed spores and result in an extension of the lag phase of outgrowth.

The inactivation mechanism is assumed to be non-changing over the observation time. This is concluded from semi-logarithmic, linear inactivation curves without tailing.

Nitrogen species of the second positive system dominated the optical emission spectrum, while oxygen species were absent or reacted with nitrogen promptly to NO_x. RNS are a fundamental inactivating component and are most likely responsible for triggering the etching of spore hulls. The RNS concentration is controlled by the plasma power density.

A slow-going diffusion of RNS in the porous material results in an over-proportional reduction of the inactivation effect as a function of the layer thickness formed by a biopolymer (starch powder or HMC film). HMC and air absorbed UV-C efficiently, and only UV-A reached the sample in the presented SMD CAPP set up.

Inactivation effects in a biopolymer matrix can be tuned by the plasma power density, but this is obviously limited to spores deposited on surfaces of a biopolymer layer. Fluidization might counteract the current limitations of the inactivation observed in fixed bed technologies.

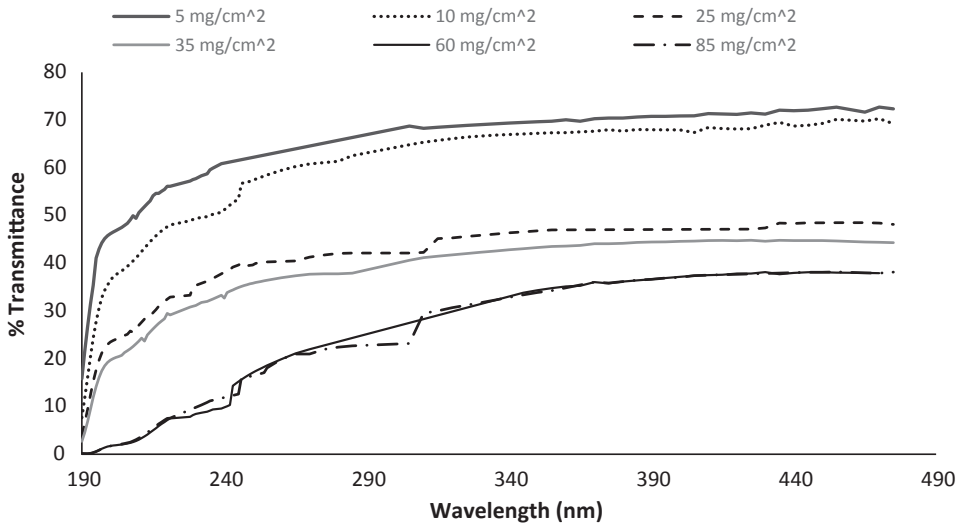

Fig. 7. Transmittance (%T) of UV-light (190–490 nm) in Hydroxymethyl-cellulose (HMC) films depending on the polymer load 5, 10, 25, 35, 60, and 85 mg/cm^2.

Acknowledgments

The present research work has been carried out with funds provided by the EC under the research and innovation program H2020 MCSA-IF EU 748314.

References

Afshari, R., & Hosseini, H. (2014). Non-thermal plasma as a new food preservation method: Its present and future prospect. *Journal of Paramedical Sciences, 5*(1), 1–6. https://doi.org/10.22037/jps.v5i1.5348.

Bárdos, L., & Baránková, H. (2010). Cold atmospheric plasma: Sources, processes, and applications. *Thin Solid Films, 518*, 6705–6713. https://doi.org/10.1016/j.tsf.2010.07.044.

Boudam, M. K., Moisan, M., Saoudi, B., Popovici, C., Gherardi, N., & Massines, F. (2006). Bacterial spore inactivation by atmospheric-pressure plasmas in the presence or absence of UV photons as obtained with the same gas mixture. *Journal of Physics D: Applied Physics, 39*(16), 3494–3507. https://doi.org/10.1088/0022-3727/39/16/S07.

Brandenburg, R., Ehlbeck, J., Stieber, M., Woedtke, Tv., Zeymer, J., & Schlüter, O. (2008). Antimicrobial treatment of heat sensitive materials by means of atmospheric pressure rf-driven plasma jet. *Contributions to Plasma Physics. 47*(1–2), 72–79. https://doi.org/10.1146/annurev.food.102308.124129.

Bußler, S. (2017). Cold atmospheric pressure plasma treatment of food matrices: Tailored modification of product properties along value-added chains of plant and animal related products. Universität Berlin, pp: 1–210. Available at: https://depositonce.tu-berlin.de/handle/11303/6144.

Butscher, D., Loon H.v., Waskow, A., Rohr, P.R.v., & Schuppler, M. (2016). Plasma inactivation of microorganisms on sprout seeds in a dielectric barrier discharge. International Journal of Food Microbiology, 238, 222-232. http://dx.doi.org/10.1016/j.ijfoodmicro.2016.09.006.

Chen, D., Peng, P., Zhou, N., Cheng, Y., Min, M., Ma, Y., ... Ruan, R. (2019). Evaluation of *Cronobacter sakazakii* inactivation and physicochemical property changes of non-fat dry milk powder by cold atmospheric plasma. *Food Chemistry, 30*(290), 270–276. https://doi.org/10.1016/j.foodchem.2019.03.149.

Cullen, P. J., Lalor, J., Scally, L., Boehm, D., Milosavljević, V., Bourke, P., & Keener, K. (2018). Translation of plasma technology from the lab to the food industry. *Plasma Processes and Polymers, 15*, 1–11. https://doi.org/10.1002/ppap.201700085.

Dababneh, B. F. (2013). An innovative MW process for microbial decontamination of spices and herbs. *African Journal of Microbiology and Research, 7*(8), 636–645. https://doi.org/10.5897/AJMR12.1487.

Deng, X., Shi, J., & Kong, M. G. (2006). Physical Mechanisms of Inactivation of *Bacillus subtilis* Spores Using Cold Atmospheric Plasmas. *IEEE Transactions on Plasma Science, 34*, 1310–1317. https://ieeexplore.ieee.org/document/1673530.

Denny, M.W. (1993). In: Princeton University Press. Air and Water: The Biology and Physics of Life's Media. New Jersey, USA. pp. 232.

EFSA (2014). Statement on the validity and robustness of information on irradiated iron oxides. EFSA Journal, 12(7), 3767, 1–11. https://doi.org/10.2903/j.efsa.2014.3767.

Farakos, S.M.S., & Frank, J.F. (2014). Challenges in the Control of Foodborne Pathogens in Low-Water Activity Foods and Spices. The Microbiological Safety of Low Water Activity Foods and Spices, 15–34. https://link.springer.com/chapter/10.1007/978-1-4939-2062-4_2.

Fiebrandt, M., Lackmann, J. W., & Stapelmann, K. (2018). From patent to product? 50 years of low-pressure plasma sterilization. *Plasma Processes and Polymers, 15*, 1–17. https://doi.org/10.1002/ppap.201800139.

Fine, F., & Gervais, P. (2004). Efficiency of Pulsed UV Light for Microbial Decontamination of Food Powders. *Journal of Food Protection, 67*(4), 787–792. https://jfoodprotection.org/doi/pdf/10.4315/0362-028X-67.4.787.

Gibson, A. M., Bratchell, N., & Roberts, T. A. (1988). Predicting microbial growth: Growth responses of salmonellae in a laboratory medium as affected by pH, sodium chloride and storage temperature. *International Journal of Food Microbiology, 6*, 155–178. https://doi.org/10.1016/0168-1605 (88)90051-7.

Guo, Y. (2013). Effects of Pulsed Light on Microbial decontamination of dry food powder. PhD thesis, University of Florida pp: 1–90. Available at: http://ufdc.ufl.edu/UFE0046406/00001.

Hertwig, C., Reineke, K., Rauh, C., & Schlüter, O. (2017). Factors involved in *Bacillus* spore' s resistance to cold atmospheric pressure plasma. *Innovative Food Science & Emerging Technologies, 43*, 173–181.

Hertwig, C., Steins, V., Reineke, K., Rademacher, A., Klocke, M., Rauh, C., & Schlüter, O. (2015). Impact surface structure and feed gas composition on *Bacillus subtilis* endospore inactivation during direct plasma treatment. *Frontiers in Microbiology, 6*, 774–786. https://www.ncbi.nlm.nih.gov/pmc/articles/PMC4526801/.

Hong, Y. F., Kang, J. G., Lee, H. Y., Uhm, H. S., Moon, E., & Park, Y. H. (2009). Sterilization effect of atmospheric plasma on *Escherichia coli* and *Bacillus subtilis* endospores. *Letters in Applied Microbiology, 48*, 33–37. https://doi.org/10.1111/j.1472-765X.2008.02480.x.

Hörmansperger, J. T., Buchmann, L., Merz, S., Schmitt, R., Beyrer, M., & Windhab, E. J. (2016). Microbial decontamination of porous model food powders by Vacuum-Steam-Vacuum treatment. *Innovative Food Science and Emerging Technologies, 34*, 367–375. https://doi.org/10.1016/j.ifset.2015.12.027.

Huang, Y., Ye, X. P., Doona, C. J., Feeherry, F. E., Radosevicha, M., & Wang, S. (2019). An investigation of inactivation mechanisms of *Bacillus amyloliquefaciens* spores in non-thermal plasma of ambient air. *Journal of Science Food Agriculture, 99*, 368–378. https://doi.org/10.1002/jsfa.9198.

Isbary, G., Shimizu, T., Li, Y. F., Stolz, W., Thomas, H. M., Morfill, G. E., & Zimmermann, J. L. (2013). Cold atmospheric plasma devices for medical issues. *Expert Reviews in Medical Devices, 10*(3), 367–377. https://doi.org/10.1586/erd.13.4.

Jeon, J., Kämpfl, T.G., Zimmermann, J.L., Morfill, G.E., & Shimizu, T. (2014). Sporicidal properties from surface micro-discharge plasma under different plasma conditions at different humidities. New Journal of Physics, 1–15. https://iopscience.iop.org/article/10.1088/1367-2630/16/10/103007.

Keener, K.M., & Misra, N.N. (2016). Chapter 14: Future of Cold Plasma in Food Processing. In: Cold Plasma in Food and Agriculture: Fundamentals and Applications, Academic Press, Ed: Misra, N.N., Schlüter, O., Cullen, P.J. 343-360. https://doi.org/10.1016/B978-0-12-801365-6.00014-7.

Kim, J. E., Lee, D. U., & Min, S. C. (2014). Microbial decontamination of red pepper powder by cold plasma. *Food Microbiology, 38*, 128–136. https://doi.org/10.1016/j.fm.2013.08.019.

Kim, J. E., Oh, Y. J., Won, M. Y., Lee, K. S., & Min, S. C. (2017). Microbial decontamination of onion powder using microwave-powered cold plasma treatments. *Food Microbiology, 62*, 112–123. https://doi.org/10.1016/j.fm.2016.10.006.

Kämpfl, T.G., Isbary, G., Shimizu, T., Li, Y.F., Zimmermann, J.L., Stolz, W., Schlegel, J., Morfill, G.E., & Schmidt, H.U. (2012). Cold Atmospheric Air Plasma Sterilization against Spores and Other Microorganisms of Clinical Interest. Applied and Environmental Microbiology, 78(15), 5077–5082. https://doi.org /10.1128/AEM.00583-12.

Li, Y. T., Shimizu, T., Zimmermann, J. L., & Morfill, G. E. (2012). Cold atmospheric plasma for surface disinfection plasma process. *Polymers, 9*, 585–589. https://doi.org/10.1002/ppap.201100090.

Mendes-Oliveira, G., Jensen, J. L., Keener, K. M., & Campanella, O. H. (2019). Modeling the inactivation of *Bacillus subtillus* spores during cold plasma sterilization. *Innovative*

Food Science and Emerging Technologies, 52, 334–342. https://doi.org/10.1016/j.isset.2018.12.011.

Mir, S. A., Shah, M. A., & Mir, M. M. (2016). Understanding the role of plasma technology in food industry. *Food and Bioprocess Technology, 9*, 734–750. https://doi.org/10.1007/s11947-016-1699-9.

Mosovská, S., Medvecká, V., Halászová, N., Durina, P., Valík, L., Mikulajová, A., & Zahoranová, A. (2018). Cold atmospheric pressure ambient air plasma inhibition of pathogenic bacteria on the surface of black pepper. *Food Research International, 106*, 862–869. https://doi.org/10.1016/j.foodres.2018.01.066.

Pankaj, S. K., Wan, Z., & Keener, K. M. (2018). Effects of cold plasma on food quality: a review. *Foods, 7*(1), 1–21. https://www.mdpi.com/2304-8158/7/1/4.

Pina-Perez, M. C., Silva-Angulo, A. B., Muguerza, B., Rodrigo, D., & Martinez, A. (2009). Synergistic effects of high hydrostatic pressure and natural antimicrobials on inactivation kinetics of *Bacillus cereus* in a liquid whole egg and skim milk mixed beverage. *Foodborne Pathogens and Disease, 6*(6), 649–656. https://doi.org/10.1089/fpd.2009.0268.

Raguse, M., Fiebrandt, M., Denis, B., Stapelmann, K., Eichenberger, P., Driks, A., ... Moeller, R. (2016). Understanding of the importance of the spore coat structure and pigmentation in the *Bacillus subtilis* spore resistance to low-pressure plasma sterilization. *Journal of Physics D: Applied Physics, 49*, 1–17. https://doi.org/10.1088/0022-3727/49/28/285401.

Sarangapani, C., Patange, A., Bourke, P., Keener, K., & Cullen, P. J. (2018). Recent advances in the application of cold plasma technology in foods. *Annual Reviews in Food Science and Technology, 25*(9), 609–629. https://www.annualreviews.org/doi/10.1146/annurev-food-030117-012517.

Setlow, P. (2007). I will survive: DNA protection in bacterial spores. *Trends in Microbiology, 15*(4), 172–180. https://doi.org/10.1016/j.tim.2007.02.004.

Shimizu, T., Zimmermann, J.L., & Morfill, G.E. (2015). Inactivation effect using surface microdischarge plasma. In: 22nd International Symposium on Plasma Chemistry July 5–10, 2015; Antwerp, Belgium. Available at: http://www.ispc-conference.org/ispcproc/ispc22/O-7-9.pdf.

Shintani, H. (2015). Major contributors to nitrogen gas plasma sterilization. *Biochemistry and Physiology, 5*(2), 1–4. https://www.omicsonline.org/open-access/major-contributors-to-nitrogen-gas-plasma-sterilization-2168-9652-1000155.php?aid=54577.

Silva-Angulo, A. B., Zanini, S. F., Rosenthal, A., Rodrigo, D., Klein, G., & Martínez, A. (2015). Comparative study of the effects of citral on the growth and injury of *Listeria innocua* and *Listeria monocytogenes* cells. *PLoS ONE, 10*(2), 1–13. https://doi.org/10.1371/journal.pone.0114026.

Singh, M. K., Ogino, A., & Nagatsu, M. (2009). Inactivation factors of spore-forming bacteria using low-pressure microwave plasmas in an N_2 and O_2 gas mixture. *New Journal of Physics, 11*, 1–16. https://doi.org/10.1088/1367-2630/11/11/115027.

Stoica, M., Alexe, P., & Mihalcea, L. (2014). Atmospheric Cold Plasma as a new strategy for foods processing – an overview. Innovative Romanian Food Biotechnology, 15, 1–8. Available at: http://www.bioaliment.ugal.ro/revista/15/paper%2015.1.pdf.

Surowsky, B., Schlüter, O., & Knorr, D. (2014). Interactions of Non-Thermal Atmospheric Pressure Plasma with Solid and Liquid Food Systems: A Review. Food Engineering Reviews, 1–27. https://link.springer.com/article/10.1007/s12393-014-9088-5.

Wallen, S. E., & Walker, H. W. (1980). Effects of Storage conditions on the resistance of *Bacillus subtilis* var. niger spores to hydrogen peroxide. *Journal of Food Science, 45*(3), 605–607. https://doi.org/10.1111/j.1365-2621.1980.tb04111.x.

Wang, S., Doona, C. J., Setlow, P., & Li, Y. Q. (2016). Characterization of cold atmospheric plasma inactivation of individual bacterial spores using Raman spectroscopy and phase contrast microscopy. *Applied and Environmental Microbiology, 82*(19), 5775–5784. https://doi.org/10.1128/AEM.01669-16.

Warda, A.K., Tempelaars, M.H., Abee, T., & Nierop Groot, M.N. (2016). Recovery of Heat Treated Bacillus cereus Spores is affected by matrix composition and factors with putative functions in damage repair. Frontiers in Microbiology, 18(7), 1096, 1–10. https://doi.org/10.3389/fmicb.2016.01096.

Yi, C., Yoon, S. Y., Eom, S., Park, S., Kim, S. B., Ryu, S., & Yoo, S. J. (2017). Self-consistent plasma chemistry model for surface microdischarge in humid air including effects of ohmic heating and gas flow. *Plasma Sources Science and Technology, 26*, 1–11. https://doi.org/10.1088/1361-6595/aa8d4e.

Zwietering, M.H., Jongenburger, I., Rombouts, F.M., & Van't Riet, K. (1990). Modeling of the Bacterial Growth Curve. Applied and Environmental Microbiology, 1875–1881. PubMed Central PMCID: PMC184525.